ARMY RESEARCH LABORATORY

Time-Accurate Simulations of Synthetic Jet-Based Flow Control for an Axisymmetric Spinning Body

by Jubaraj Sahu

ARL-TR-3300 **September 2004**

NOTICES

Disclaimers

The findings in this report are not to be construed as an official Department of the Army position unless so designated by other authorized documents.

Citation of manufacturer's or trade names does not constitute an official endorsement or approval of the use thereof.

DESTRUCTION NOTICE—Destroy this report when it is no longer needed. Do not return it to the originator.

Army Research Laboratory
Aberdeen Proving Ground, MD 21005-5066

ARL-TR-3300 **September 2004**

Time-Accurate Simulations of Synthetic Jet-Based Flow Control for an Axisymmetric Spinning Body

Jubaraj Sahu
Weapons and Materials Research Directorate, ARL

REPORT DOCUMENTATION PAGE

Form Approved
OMB No. 0704-0188

1. REPORT DATE *(DD-MM-YYYY)*	2. REPORT TYPE	3. DATES COVERED (From - To)
September 2004	Final	October 2001 to December 2003

4. TITLE AND SUBTITLE

Time-Accurate Simulations of Synthetic Jet-Based Flow Control for an Axisymmetric Spinning Body

5a. CONTRACT NUMBER

5b. GRANT NUMBER

5c. PROGRAM ELEMENT NUMBER

6. AUTHOR(S)

Jubaraj Sahu (ARL)

5d. PROJECT NUMBER
1L1622618.A

5e. TASK NUMBER

5f. WORK UNIT NUMBER

7. PERFORMING ORGANIZATION NAME(S) AND ADDRESS(ES)

U.S. Army Research Laboratory
Weapons and Materials Research Directorate
Aberdeen Proving Ground, MD 21005-5066

8. PERFORMING ORGANIZATION REPORT NUMBER

ARL-TR-3300

9. SPONSORING/MONITORING AGENCY NAME(S) AND ADDRESS(ES)

10. SPONSOR/MONITOR'S ACRONYM(S)

11. SPONSOR/MONITOR'S REPORT NUMBER(S)

12. DISTRIBUTION/AVAILABILITY STATEMENT

Approved for public release; distribution is unlimited.

13. SUPPLEMENTARY NOTES

14. ABSTRACT

This report describes a computational study undertaken to consider the aerodynamic effect of synthetic jets as a means of providing the control authority needed to maneuver a projectile at a low subsonic speed. A time-accurate Navier-Stokes computational technique has been used to obtain numerical solutions for the unsteady jet-interaction flow field for a spinning projectile at a subsonic speed, Mach = 0.24, and angle of attack, 0 degree. Numerical solutions have been obtained by Reynolds-averaged Navier-Stokes (RANS) and hybrid RANS-large-eddy simulation turbulence models. Unsteady numerical results show the effect of the jet on the flow field and the aerodynamic coefficients, particularly the lift force. These numerical results are being used to assess if synthetic jets can be used to provide the control authority needed for maneuvering munitions to hit the targets with precision.

15. SUBJECT TERMS

flow control; projectile aerodynamics; spinning; synthetic jet; unsteady

16. SECURITY CLASSIFICATION OF:			17. LIMITATION OF ABSTRACT	18. NUMBER OF PAGES	19a. NAME OF RESPONSIBLE PERSON
a. REPORT	b. ABSTRACT	c. THIS PAGE			Jubaraj Sahu
Unclassified	Unclassified	Unclassified	UL	30	19b. TELEPHONE NUMBER (*Include area code*) 410-278-3707

Contents

List of Figures

Acknowledgments

This work was accomplished as part of a research project on micro-adaptive flow control sponsored and jointly funded by the Defense Advanced Research Projects Agency (DARPA) and the U.S. Army Research Laboratory (ARL). The author wishes to thank Sukumar Chakravarthy from Metacomp Technologies for his expert technical advice. The scientific visualization work of Richard Angelini of ARL and the computational support of the ARL Major Shared Resource Center are greatly appreciated.

INTENTIONALLY LEFT BLANK

1. Introduction

The prediction of aerodynamic coefficients for projectile configurations is essential in the assessment of the performance of new designs. Accurate determination of aerodynamics is critical to the low-cost development of new, advanced guided projectiles, rockets, missiles, and smart munitions. Fins, canards, and jets can be used to provide control for maneuvering projectiles and missiles. The flow fields associated with these control mechanisms for the Army weapons are complex, involving three-dimensional (3-D) shock-boundary layer interactions, jet interaction with the free stream flow, and highly viscous dominated separated flow regions (*1 through 3*). The jet interference can extend over significant portions of the projectile and must be modeled correctly. For missiles, jet thrusters have been studied over a number of years to provide high-speed aerodynamic control. These thrusters interact with the surrounding flow field, and the resulting jet interaction flow field again is complex. Recently, several studies have shown that tiny synthetic unsteady jets can significantly alter the flow field and pressure distributions for airfoils and cylinders (*4,5,6*). These synthetic jets are active control devices with zero net mass flux and are intended to produce the desired control of the flow field through momentum effects. Many parameters such as jet location, jet velocity, and actuator frequency can affect the flow control phenomenon.

Smith and Glezer (*4*) have conducted an excellent study of the flow control by synthetic jets to provide increased fundamental understanding of the flow physics. Amitay et al. (*5*) experimentally investigated flow separation control on a cylinder using synthetic jet actuators. Their work showed that the interaction of the synthetic jet with the free stream flow resulted in a virtual modification of the body shape and significantly increased the lift force as a result of the flow reattachment. Aerodynamic flow control over an unconventional airfoil has also been demonstrated by Amitay et al. (*6*) to enhance post-stall performance via actuators operating at frequencies higher than the characteristic frequency of the airfoil. The synthetic jets are also being investigated for possible applications to improve heat transfer, reduce drag, and enhance mixing (*7*) in combustors, etc. The present analysis involves these synthetic jets for projectile aerodynamic control. The emphasis in the present research is to provide insight into the interaction of these unsteady jets with the free stream flow and to determine the feasibility of these jets for aerodynamic control of a subsonic spinning projectile.

Computational and experimental data for these jet interactions are very limited. Simple theories cannot predict the complex flow fields associated with the jet interaction, and experimental tests are very expensive. To help reduce experimental costs, computational fluid dynamics (CFD) are being used to predict these complex flows and provide detailed pressure, force, and moment data. There have been several recent numerical studies (*8,9*) of flow separation control using synthetic jet actuators. He and Kral (*8*) have used Reynolds-averaged Navier-Stokes (RANS)

models to study the effect of jet location and jet-forcing frequency on the lift and drag forces on an airfoil. The jet actuator was shown to increase the time-averaged lift and also to increase the amplitude of oscillation. Lee and Goldstein (*9*) have used the direct numerical simulation (DNS) to model a two-dimensional (2-D) synthetic jet. Although this simulation produced very good results, the application of DNS to practical 3-D flows of interest is prohibitive because of its computing resources requirement. Even large-eddy simulations (LES) (*10*) where large eddies are computed directly and the small scales are modeled require large computational cost compared to RANS simulations. While the RANS method works well for steady flows, the accuracy of this method for unsteady flows may be less than desired. Since the large energy-containing eddies are computed by the LES method, this technique is more capable of handling unsteady shear layers and wakes, etc. Recently, therefore, a hybrid approach (*11,12*) that combines RANS and LES has been developed to solve practical problems of interest involving unsteady flows at reasonable computational cost. Both RANS and hybrid RANS-LES models have been used in the present study.

The advanced CFD capability used here solves the Navier-Stokes equations (*13 through 16*) and incorporates unsteady boundary conditions for simulation of the synthetic jets (*17,18*). Also, a hybrid RANS-LES turbulence model (*12*) was used for accurate numerical prediction of unsteady jet flows. Sahu (*19*) used these advanced techniques and performed numerical flow field computations for steady and unsteady jets for a non-spinning projectile configuration at a low subsonic speed. Computed lift forces attributable to the unsteady synthetic jets were found to match the experimental data well (*17,18*). The present numerical study is a direct extension of that research to a spinning projectile at subsonic speeds and atmospheric flight conditions. The following sections describe the numerical procedure and the computed results obtained. Results obtained for the spinning projectile configuration are presented at Mach 0.24, angle of attack 0 degree, and a spin rate of 67 Hz.

2. Solution Technique

2.1 CFD++ Flow Solver

The complete set of 3-D time-dependent Navier-Stokes equations is solved in a time-accurate manner for simulations of unsteady jets. A commercially available code, CFD++ (*14,15,16*), is used for the time-accurate unsteady CFD simulations. The basic numerical framework in the code contains unified grid, unified physics, and unified computing features. The user is referred to these references for details of the basic numerical framework. Here, only a brief synopsis of this framework and methodology is given.

The 3-D, time-dependent RANS equations are solved by the following finite volume method:

$$\frac{\partial}{\partial t}\int_V \mathbf{W}dV + \oint[\mathbf{F}-\mathbf{G}]\cdot dA = \int_V \mathbf{H}dV \tag{1}$$

in which **W** is the vector of conservative variables, **F** and **G** are the inviscid and viscous flux vectors, respectively, **H** is the vector of source terms, V is the cell volume, and A is the surface area of the cell face.

For low speed flows considered here, "preconditioned implicit relaxation" scheme is used to achieve faster convergence. It combines three basic ideas: (1) implicit local time stepping, (2) relaxation, and (3) preconditioning. Preconditioning the equations ideally equalizes the eigenvalues of the inviscid flux Jacobians and removes the stiffness arising from large discrepancies between the flow and sound velocities at low speeds. The use of an implicit scheme circumvents the stringent stability limits suffered by their explicit counterparts, and successive relaxation allows cells to be revised as information becomes available and thus aids convergence. These features of the code have been extremely useful in the present numerical simulations at very low subsonic speeds. Second order discretization was used for the flow variables and the turbulent viscosity equation. The turbulence closure is based on topology-parameter-free formulations. Two-equation and higher order hybrid RANS-LES turbulence models were used for the computation of turbulent flows. These models are ideally suited to unstructured bookkeeping and massively parallel processing because of their independence from constraints related to the placement of boundaries and/or zonal interfaces.

For computations of unsteady jet interaction flow fields that are of interest here, dual time stepping (as described next) was used to achieve the desired time accuracy. In addition, special jet boundary conditions were developed and used for numerical modeling of synthetic jets. Grid was actually moved to take into account the spinning motion of the projectile.

2.2 Dual Time Stepping

The "dual time-stepping mode" of the code was used to perform the transient flow simulations. The term "dual time step" implies the use of two time steps. The first is an "outer" or global (and physical) time step that corresponds to the time discretization of the physical time variation term. This time step can be chosen directly by the user and is typically set to a value to represent 1/100 of the period of oscillation expected or forced in the transient flow. This time step is applied to every cell (not separately varying).

An artificial or "inner" or "local" time variation term is added to the basic physical equations. This time step and corresponding "inner iteration" strategy is chosen to help satisfy the physical transient equations to the desired degree. If the inner iterations converge, then the outer physical transient equations (their discretization) are satisfied exactly; otherwise, approximately. For the inner iterations, the time step is allowed to vary spatially. Also, relaxation with multi-grid (algebraic) acceleration is employed to reduce the residues of the physical transient equations. It is found that an order of magnitude reduction in the residues is usually sufficient to produce a

good transient iteration. This may require a few internal iterations to achieve (between 3 and 10, depending on the magnitude of the outer time step), the nature of the problem, the nature of the boundary conditions, and the consistency of the mesh with respect to the physics at hand.

2.3 Unsteady Jet Boundary Condition

A large number of boundary conditions (BC) are available and can be specified at the appropriate boundaries. Each boundary condition is encoded as a basic form along with a collection of modifiers. One particular BC used for the simulations presented here is a "oscillating jet" BC. In its basic form, it is a steady inflow/outflow BC wherein the user supplies the velocity normal to the boundary along with static temperature and any turbulence quantities. When the velocity provided is negative, it is considered to be an inflow and when it is positive, it is treated as an outflow. In the case of inflow, the static temperature and turbulence quantities are used along with the inflow velocity. In the case of outflow, only the velocity is used. At inflow, the tangential component of velocity is set to zero, and at outflow, the tangential component is extrapolated from the interior. At outflow, all primitive variables except normal velocity are extrapolated from the interior. At inflow, the static pressure is taken from the interior.

The first modifier available for this BC allows the velocity to oscillate. The base velocity is multiplied by an amplitude which varies as sin ($2\pi ft$) where f is the frequency of the oscillation. Thus, the oscillating velocity can cycle from being positive to being negative and back within each period (or from being negative to positive and back, based on the sign of the input for the basic BC formulation).

A second modifier permits the steady or oscillating inflow/outflow to be "on" over certain time intervals and "off" during other intervals. During "on" periods, the basic or the basic multiplied by the oscillating amplitude multiplier (first modifier) is used. The user provides the ranges of time during which the jet is on. The user also provides a repetition time period (e.g., the time period corresponding to one spin rotation of the projectile). Within each time period, therefore, there are sets of starting and ending times that define when the jet is on. During "off" periods, the amplitude is set to zero. In parts of the cycle when the jet is off, the boundary condition thus reverts to the condition of inviscid surface tangency. This allows the flow to slip past the boundary, as would exist (in the form of a shear layer) if the jet were emanating from a cavity/hole.

2.4 Grid Movement

CFD++ code has many features related to grid movement. Grid velocity can be assigned to each mesh point. This general capability can be tailored for many specific situations. For example, the grid point velocities can be specified to correspond to a spinning projectile. In this case, the grid speeds are assigned as if the grid were attached to the projectile and spinning with it.

A proper treatment of grid motion requires careful attention to the details of the implementation of the algorithm applied to every mesh point and mesh cell so that no spurious numerical effects are created. For example, a required consistency condition is that free stream uniform flow be preserved for arbitrary meshes and arbitrary mesh velocities. This condition is satisfied in the code.

Another important aspect concerns the way that boundary conditions are affected by grid velocities. Two significant classes of boundary conditions (slip or no slip at a wall, and far field boundary) are considered here. Both are treated in a manner that works seamlessly with or without mesh velocities. In both cases, consider the contra-variant velocity, which includes the effect of grid motion. Effectively, it is the normal component of the velocity relative to the mesh. At the body surface, it is set to zero. For a no-slip wall, one adds the requirement that the tangential component of the velocity is equal to the mesh velocity by default. Effectively, this assures that the velocity of the mesh is equal to the velocity of the flow at the body. At a far-field boundary, the sign of the contra-variant velocity determines inflow (negative sign) or outflow (positive sign). The magnitude of the contra-variant velocity is compared with the local speed of sound, helping to define one of four possibilities: supersonic inflow, supersonic outflow, subsonic inflow, subsonic outflow. The characteristics theory is used to determine what and how much information is applied as the boundary condition for each type. A careful treatment of the grid motion results in its use in a transparent manner.

2.5 Hybrid RANS-LES Model

Currently, the two most popular forms of turbulence closure, namely, ensemble-averaged models (typically based on the RANS equations) and LES with a sub-grid-scale model, both face a number of unresolved difficulties. Specifically, existing LES models have met with problems related to the accurate resolution of the near-wall turbulent stresses. In the near-wall region, the foundations of large-eddy simulation are less secure, since the sizes of the (anisotropic) near-wall eddies approach those of the Kolmogorov scale, requiring a mesh resolution approaching that of a direct numerical simulation. On the other hand, existing ensemble-averaged turbulence models are limited by their empirical calibration. Their representation of small-scale flow physics cannot be improved by mesh refinement, and over short time scales, they tend to be overly dissipative with respect to perturbations around the mean, often suppressing unsteady motion altogether.

While LES is an increasingly powerful tool for unsteady turbulent flow prediction, it is still prohibitively expensive. To bring LES closer to becoming a design tool, a hybrid RANS-LES approach based on limited numerical scales (LNS) has been recently developed by Metacomp Technologies (*12*). This approach combines the best features of RANS and LES in a single modeling framework. The LNS model is formulated from an algebraic or differential Reynolds-stress model, in which the sub-grid stresses are limited by the numerically computed local length scale and velocity scale products. LNS thus behaves like its parent RANS model on RANS-type

grids but reverts to an *anisotropic* LES sub-grid model as the mesh is refined locally, thereby reaching the correct (DNS) fine grid limit. Locally embedded regions of LES may be achieved automatically through local grid refinement, while the superior near-wall stress predictions of the RANS model are preserved, removing the need of *ad hoc*, topography-parameter-based wall damping.

The LNS hybrid formulation is well suited to the simulation of unsteady flows, including mixing flows, and contains no additional empirical constants beyond those appearing in the original RANS and LES sub-grid models. With this method, a regular RANS-type grid is used except in isolated flow regions where denser, LES-type mesh is used to resolve critical unsteady flow features. The hybrid model transitions smoothly between an LES calculation and a cubic k-ε model, depending on grid fineness. A somewhat finer grid was placed around the body and near the jet, but the rest of the flow field was occupied by a coarser, RANS-like mesh.

To date, the LNS technique has been used successfully on a number of unsteady flows. Examples include flows over cavities, flows around blunt bodies, flows around airfoils and wings at high angle of attack, separation suppression using synthetic jets, forced and natural convection flows in a room, and mixing flows in nozzles.

3. Results and Discussion

Time-accurate unsteady numerical computations using viscous Navier-Stokes methods were performed to predict the flow field and aerodynamic coefficients on the subsonic projectile for jet-on conditions. Three-dimensional numerical computations have been performed for the projectile configuration with jet interaction with CFD++ code at a subsonic Mach number of 0.24, angle of attack 0 degree, and a spin rate of 67 Hz. The preconditioned version of the CFD++ code was used to obtain an efficient numerical solution at low speed. For modeling of the unsteady synthetic jets, both unsteady RANS and a hybrid RANS-LES approach (*12*) were used. For computations of these unsteady jets, full 3-D computations are performed and no symmetry was used.

The subsonic projectile is a 1.8-caliber ogive-cylinder configuration (see figure 1). Here, the primary interest is in the development and application of CFD techniques for accurate simulation of projectile flow field in the presence of unsteady jets. The first step here was to obtain the steady state results for the same projectile without the jet. The converged jet-off steady state solution was then used as the starting condition for the computation of time-accurate unsteady flow field for the projectile with synthetic jets. Computations were also performed for the steady jet cases. The jet locations on the projectile are shown in figure 2. The jet conditions were specified at the exit of the jet for both steady (fixed jet velocity) and unsteady (sinusoidal variation in jet velocity) jets. The jet conditions specified include the jet pressure, density, and

velocity components. The flow field inside the tiny jet cavity is not computed. For the unsteady jet case, time-dependent jet boundary conditions are applied at the jet exit. Numerical computations have been made for these jet cases at a Mach number, M = 0.24, an angle of attack, $\alpha = 0$ degree, and a spin rate of 67 Hz. The jet width was 0.32 mm, the jet slot half-angle was 18 degrees, and the peak jet velocities used were 31 and 69 m/s operating at a frequency of 1000 Hz.

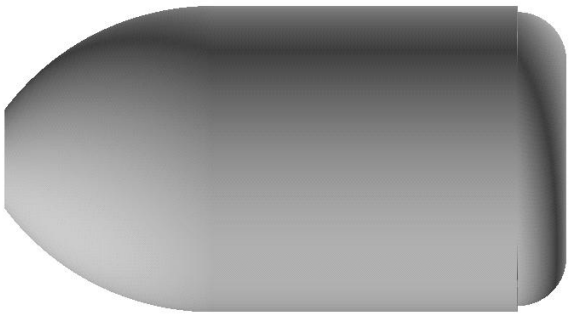

Figure 1. Projectile geometry.

Figure 2. Aft-end geometry showing the jet location.

A computational grid expanded near the vicinity of the projectile is shown in figure 3. Grid points are clustered near the jet as well as the boundary layer regions to capture the high gradient flow regions. The computational grid has 211 points in the streamwise direction, 241 in the circumferential direction, and 80 in the normal direction. The unsteady simulation took thousands of hours of central processing unit time on a Silicon Graphics (SGI) Origin computer running with 16 to 32 processors.

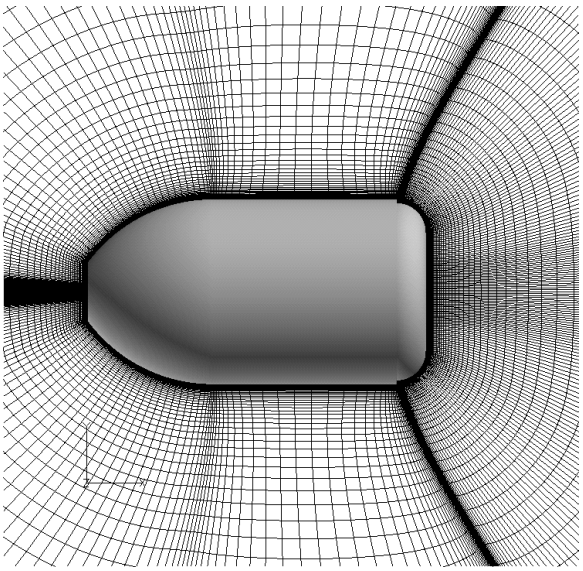

Figure 3. Computational grid near the projectile.

Unsteady time-accurate CFD computations require huge computer resources. All the results presented here were obtained from unsteady numerical computations with a single synthetic jet on a 40–mm subsonic grenade (figure 1). Looking from the front (see figure 4), the projectile spins clockwise at a rate of 67 Hz. The jet actuation corresponds to one-fourth of the spin cycle from -45 to +45 degrees with 0 degree being the positive y-axis. The jet is off during the remaining three-fourths of the spin cycle. Time-accurate unsteady simulation even with a single synthetic jet requires a large amount of resources. The unsteady CFD modeling technique required about 600 time steps to resolve a full spin cycle. The unsteady synthetic jet operates at a high frequency of 1000 Hz. For the part of the spin cycle when the jet is on, the jet operated for approximately for four cycles. Time-accurate CFD modeling of each jet cycle required more than 40 time steps. The actual computing time for one full spin cycle of the projectile was about 50 hours using 16 processors (i.e., 800 processor-hours) on an SGI Origin 3000 or an IBM SP3 system for a mesh size about 4,000,000 grid points. Multiple spin cycles and thus, a large number of synthetic jet operations were required to reach the desired periodic time-accurate unsteady result. As will be seen later, some cases were run for as many as 60 spin cycles, requiring more than 48,000 processor hours of computer time. Many flow field solutions were saved at regular intermittent time intervals to produce “movies” to gain insight into the physical phenomenon resulting from the synthetic jet interactions. Computed particle traces emanating from the jet into the wake are shown in figure 5 at a given instant in time for M = 0.24 and $\alpha = 0$ degree. These traces are colored by the velocity magnitude. The particle traces emanating from the jet interact with the wake flow, making it highly unsteady. It shows the flow in the base region to be asymmetric because of the interaction of the unsteady jet. The shear layer from the free stream flow resulting from the step corner up stream from the base interacts with the unsteady jet and deteriorates just a short distance down stream from the jet. The unsteady jet substantially alters the flow field near the jet and the base region, which in turn affected the forces and moments even at 0 degree angle of attack.

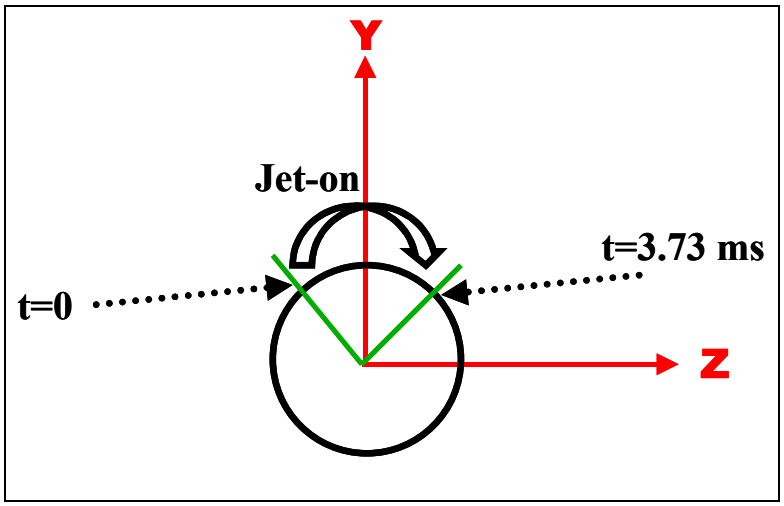

Figure 4. Schematic showing the jet actuation in one spin cycle (view from the front or nose).

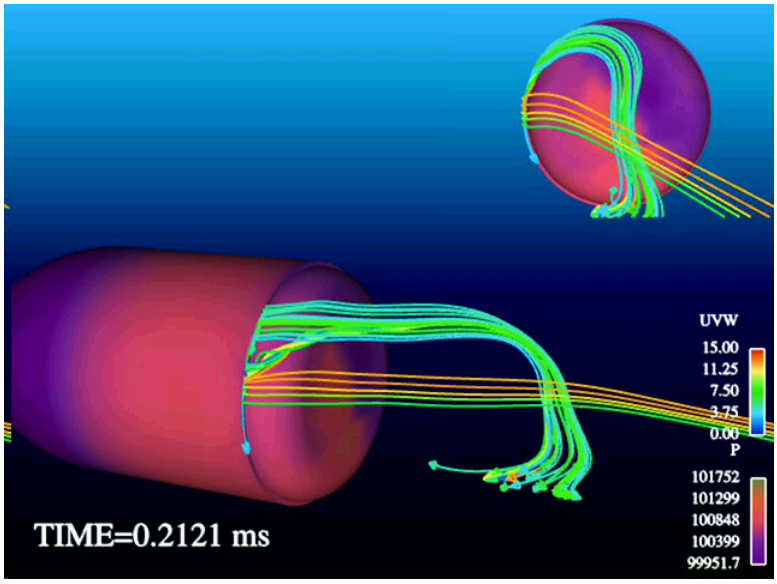

Figure 5. Computed particle traces colored by velocity, jet on, M = 0.24, α = 0 degree.

The computed surface pressures from the unsteady flow fields are integrated to obtain the aerodynamic forces and moments. Computed results have been obtained with unsteady RANS (URANS) as well as the hybrid RANS-LES approach referred here as the LNS for the jet-on conditions. The unsteady jet is applied while the projectile is spinning. For comparison, the jet-off computations have been performed in a time-accurate mode with the LNS model. Also, the jet-off URANS calculations were first obtained and the jets were activated, beginning at time, t = 28 ms. The computed normal or lift force (F_Y) and side force (F_Z) are shown in figures 6 and 7 as a function of time for two different jet velocities, 31 and 69 m/s, respectively. These computed results clearly indicate the unsteady nature of the flow field. These forces are found to

change as a function of time. Changes in the side force are slightly smaller than changes in the lift force. As shown in figure 6, URANS calculations clearly show the effect of the jet on the lift and side forces. When the jet is turned off, the levels of these forces drop to the same levels before the jet activation corresponding to the jet-off wake flow. Similar behavior can be seen in figure 7 for the bigger jet case. The effect of the jet is stronger, as evidenced by the larger peak magnitudes seen in the forces.

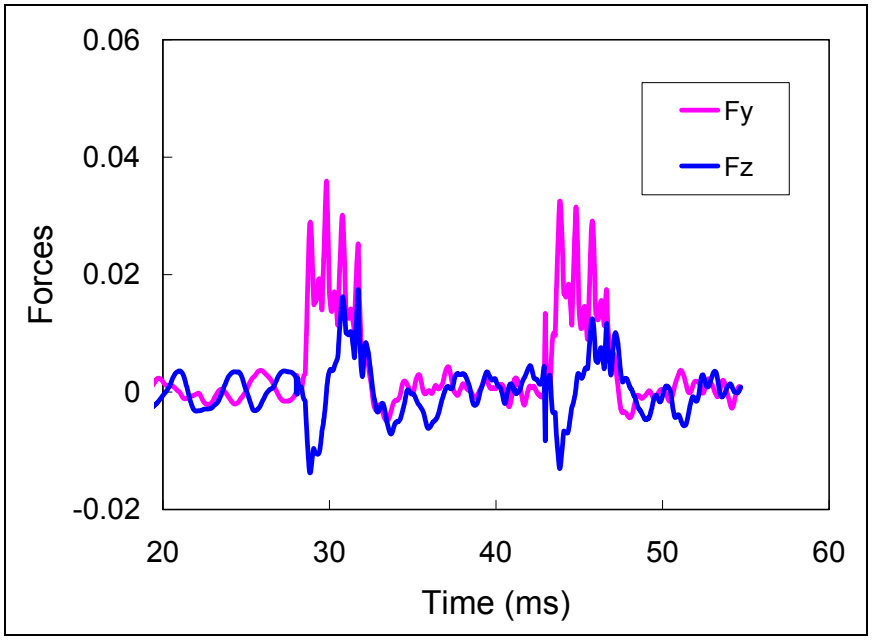

Figure 6. Computed lift and side forces, jet on, URANS, M = 0.24, jet velocity = 31 m/s, α = 0 degree.

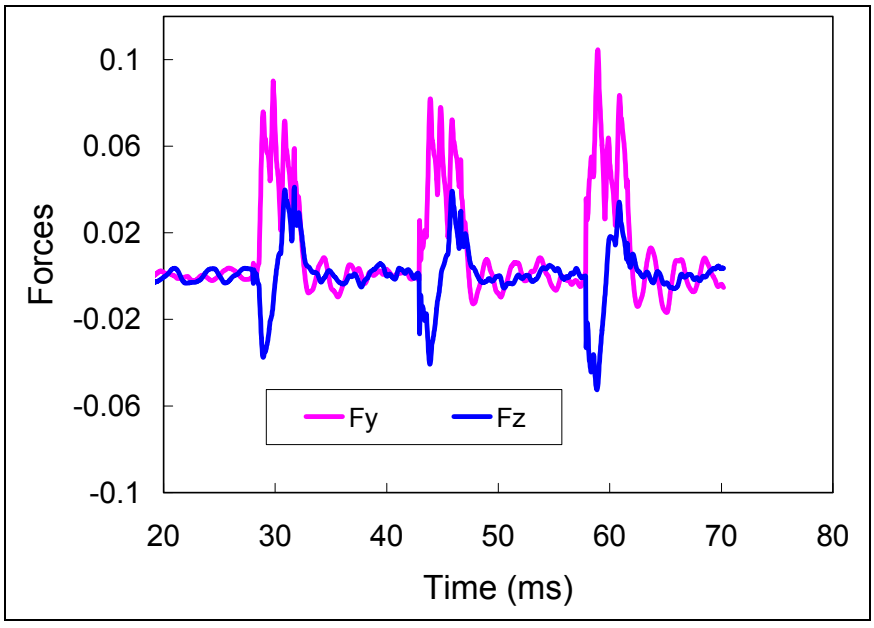

Figure 7. Computed lift and side forces, jet on, URANS, M = 0.24, jet velocity = 69 m/s, α = 0 degree.

Computed results were also obtained with the hybrid RANS-LES or LNS approach for the jet-on conditions. Figure 8 shows the lift and side forces obtained with LNS as a function of time for the bigger jet case. Here again, the jet was turned on at time, t = 28 ms, starting with an URANS solution. The mean values of both F_Y and F_Z forces are non-zero because of the jet interaction. The LNS model predicts large amplitudes of oscillations in the forces. For comparison purposes, jet-off calculations were obtained with the LNS model, starting with the same initial URANS solution. A comparison of the computed lift force with LNS for jet-off and jet-on conditions (see figure 9) clearly indicates that the wake is unsteady. Also, the amplitudes of oscillations are large for jet-off and jet-on cases. Figure 10 shows the comparison of the predicted lift force with URANS and LNS models. As indicated earlier, the URANS approach clearly shows when the jet is on and when it is off during the spin cycle. The effect caused by the jet for the LNS case is not as easily seen. It is hidden in these oscillations. However, the mean value of the lift force seems to be close to zero when the jet is off during the spin cycle. In general, the levels of the lift force oscillations predicted by the LNS models are larger than those predicted by the URANS.

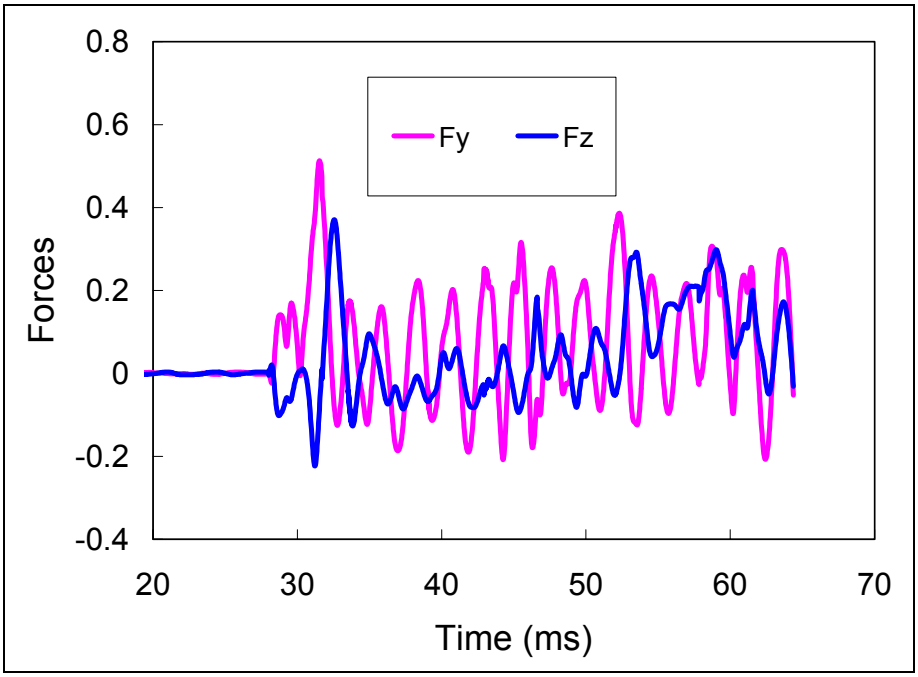

Figure 8. Computed lift and side forces, jet-on, LNS, M = 0.24, jet velocity = 69 m/s, α = 0 degree.

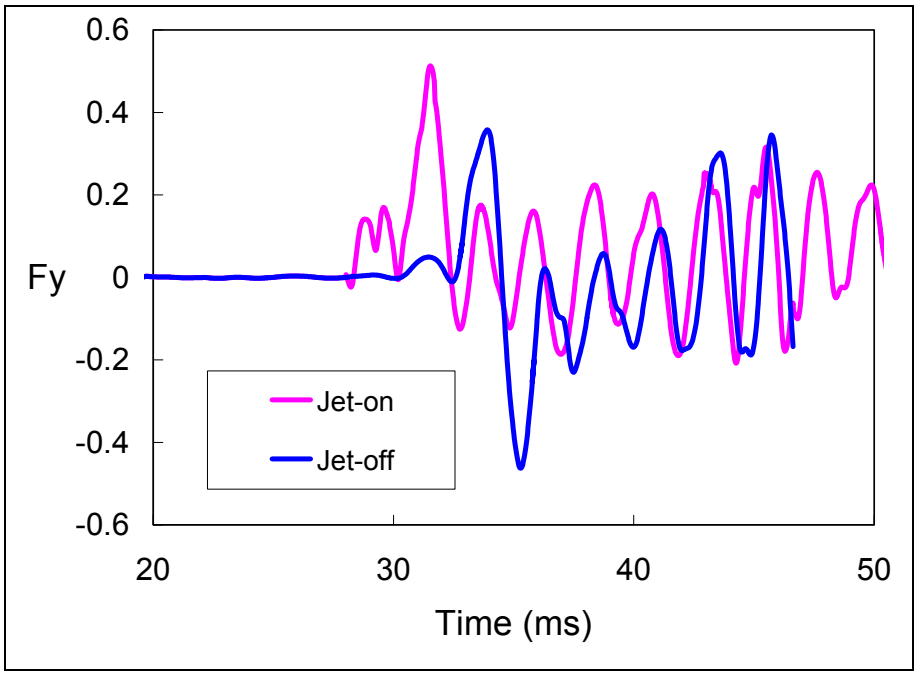

Figure 9. Comparison of computed lift force, jet-off and jet-on (jet velocity = 69 m/s), LNS, M = 0.24, α = 0 degree.

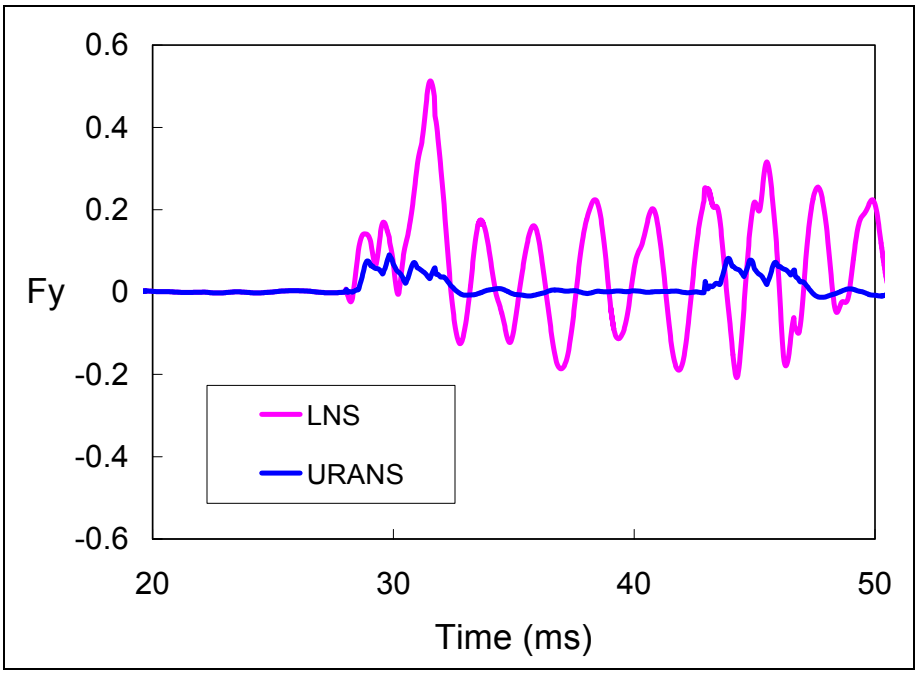

Figure 10. Comparison of computed lift force, URANS and LNS, M = 0.24, jet velocity = 69 m/s, α = 0 degree.

Based on the comparisons for the non-spinning cases, the LNS method predicted the level of forces that closely matched the data (*19*). In the current study, the addition of spin as well as the jet actuation for part of the spin cycle further complicates the analysis of the CFD results with LNS. Whether the jet is on or off, the level of oscillations seen is quite large and the effect of the jet cannot be easily seen in the instantaneous time histories of the unsteady forces and moments. To get the net effect of the jet, unsteady computations were run for many spin cycles of the projectile both with and without the synthetic jets. For the synthetic jet cases, two jet velocities of 31 and 69 m/s (peak values) were used. The CFD results are plotted over only one spin cycle; each subsequent spin cycle was superimposed and a time-averaged result is then obtained over one spin cycle. In all these cases, the jet is on for one-fourth of the spin cycle (time, t = 0 to 3.73 ms) and is off for the remainder (three-fourths) of the spin cycle. Figures 11 through 15 show the time-averaged results over a spin cycle. Figure 11 shows the averaged computed lift force for the jet-off case after 5, 10, 15, and 20 spin cycles, and as expected, it is close to zero, especially after 20 spin cycles.

Figure 12 shows the computed lift force again averaged over many spin cycles for the peak jet velocity of 31 m/s. The jet effect can clearly be seen when the jet is on (t = 0 to 3.73 ms) even after 5 or 10 spin cycles. The net lift is ~0.07 newton because of the jet actuation and seems to have converged after 20 spin cycles. For the remainder of the spin cycle, the jet is off; however, the effect of the jet on the wake still persists, and this figure shows that lift force is still available because of the jet interaction. The magnitude of the lift force is, of course, reduced when the jet is off. The force and moment results for a bigger jet (peak jet velocity of 69 m/s) are shown in figures 13 and 14, respectively. As shown in figure 13, the lift force requires at least five spin cycles before reaching a more consistent level. The lift force is on the order of 0.17 when the jet is on (t = 0 to about 4 ms), and then decreases gradually. The mean level of the lift force when the jet is off during the spin cycle is on the order of 0.07 newton. The variation in the pitching moment (see figure 14) is very similar and seems to settle after 20 spin cycles. Figure 15 shows the computed averaged lift force after 50 and 60 spin cycles for jet velocities 31 and 69 m/s, respectively. It clearly shows that the larger jet produces larger lift force than the smaller jet when the jet is activated. Again, one can see a contribution of the jet to the lift force for both cases, even when the jet is off (time from 4 to 15 ms). The lift force can be integrated over time to obtain the impulse. Figure 16 shows the impulse obtained from the lift force as a function of the spin cycles for both jets. As seen here, in both cases, it takes about 30 to 40 spin cycles before the impulse achieves an asymptote at a fixed value. The impulse is larger for the larger jet. Figure 17 shows the impulse obtained from both the lift force and the side force for the larger jet case. The impulse from the side force drops close to zero at about 30 spin cycles, then rises somewhat, and reaches an asymptote at a value slightly higher than zero.

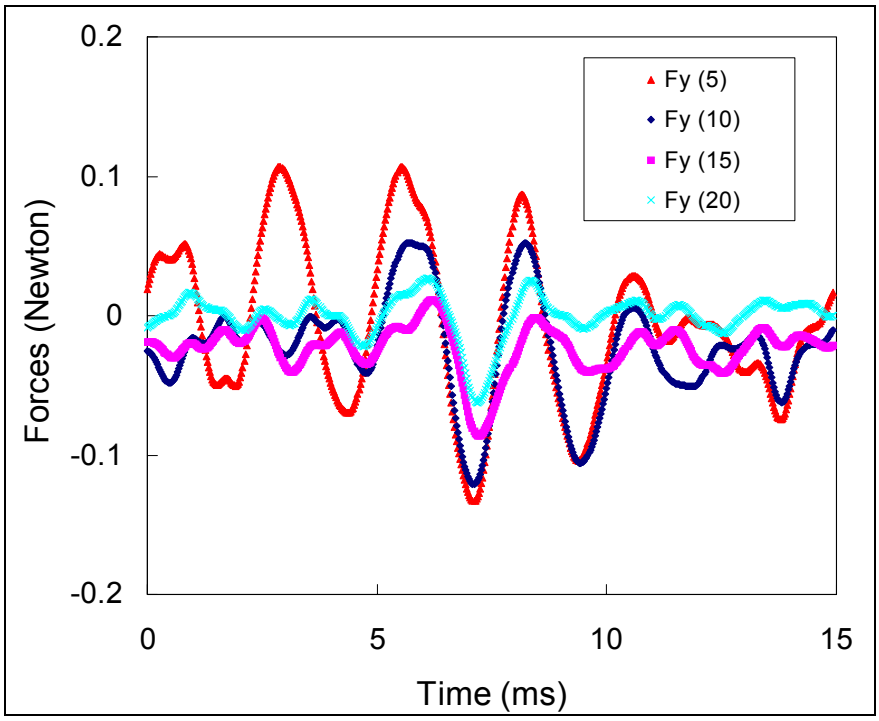

Figure 11. Computed lift force over many spin cycles, jet-off, LNS, M = 0.24, α = 0 degree, spin = 67 Hz.

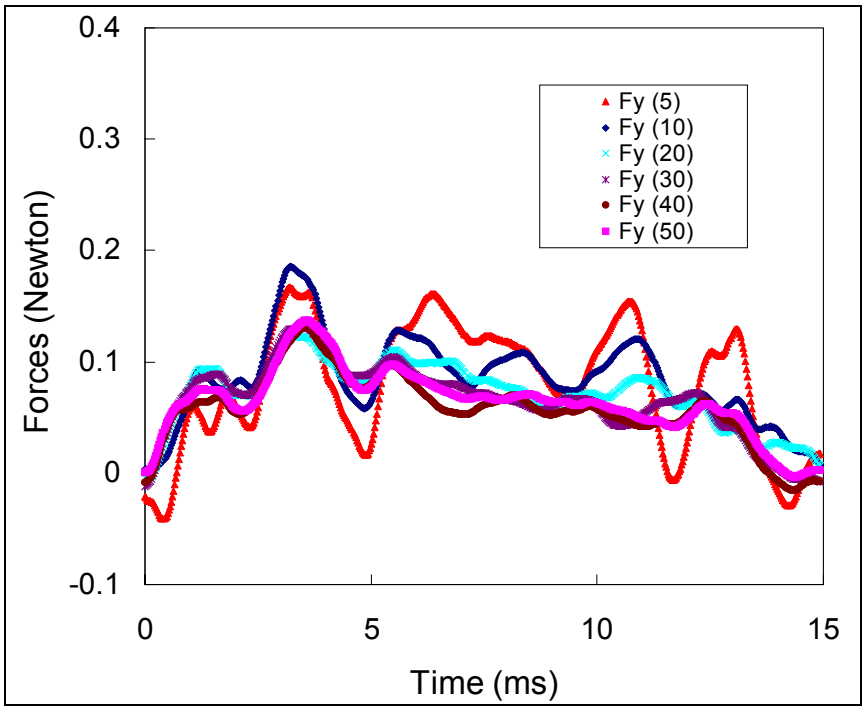

Figure 12. Computed lift force over many spin cycles, LNS, jet velocity = 31 m/s, M = 0.24, α = 0 degree, spin = 67 Hz.

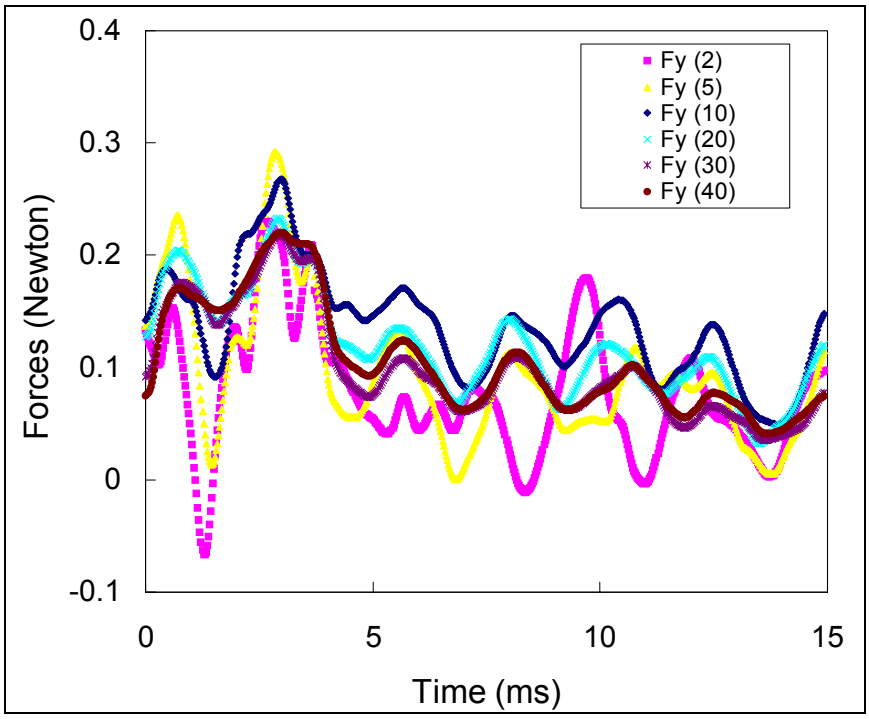

Figure 13. Computed lift force over many spin cycles, LNS, jet velocity = 69 m/s, M = 0.24, α = 0 degree, spin = 67 Hz.

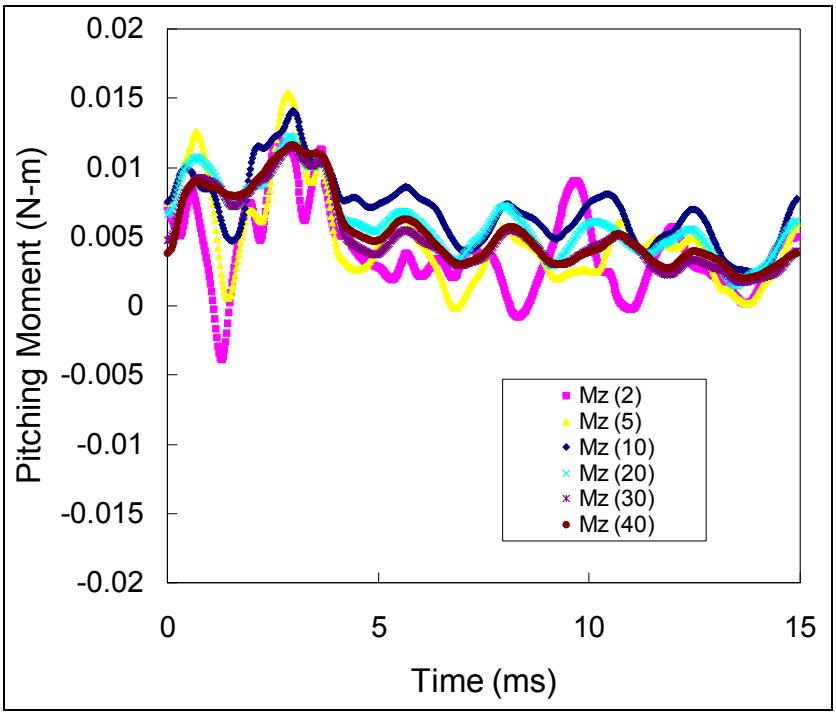

Figure 14. Computed pitching moment over many spin cycles, LNS, jet velocity =69 m/s, M = 0.24, α = 0 degree, spin = 67 Hz.

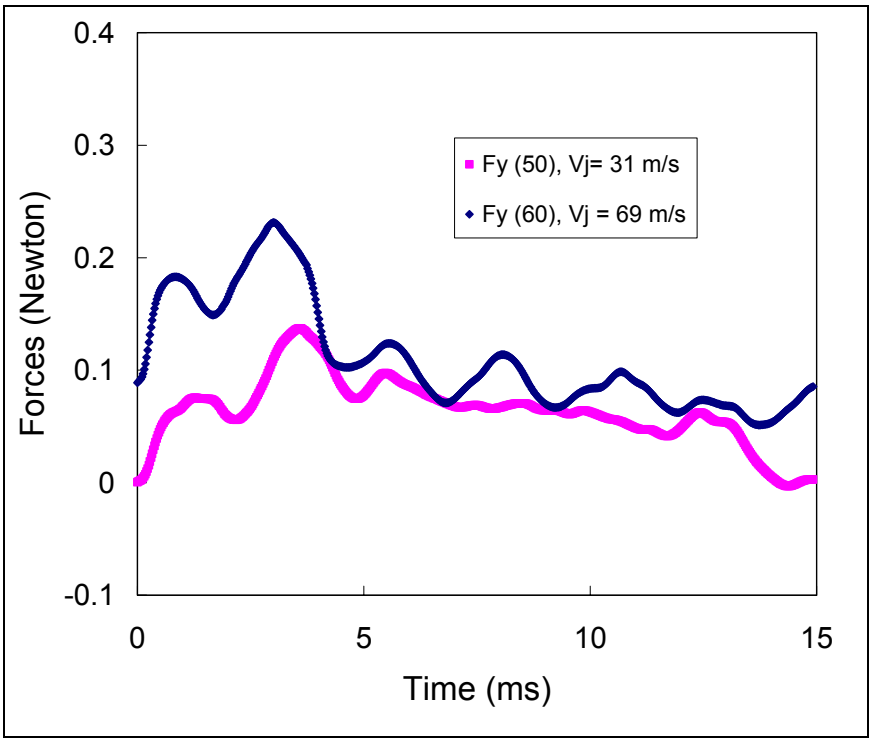

Figure 15. Computed lift force over many spin cycles for different jet velocities, LNS, M = 0.24, α = 0 degree, spin = 67 Hz.

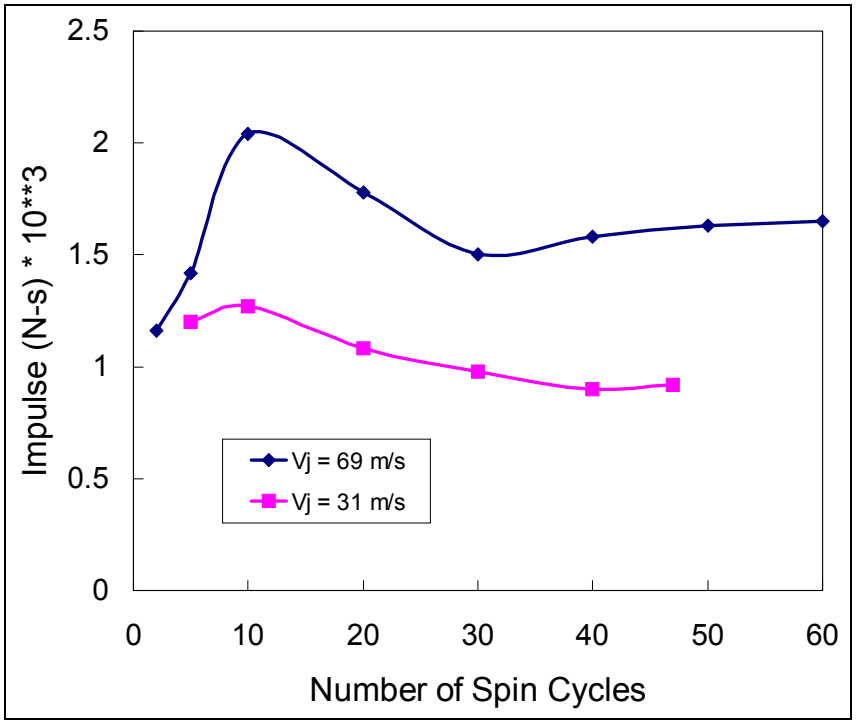

Figure 16. Computed impulse from the lift force as a function of spin cycles for different jet velocities, LNS, M = 0.24, α = 0 degree, spin = 67 Hz.

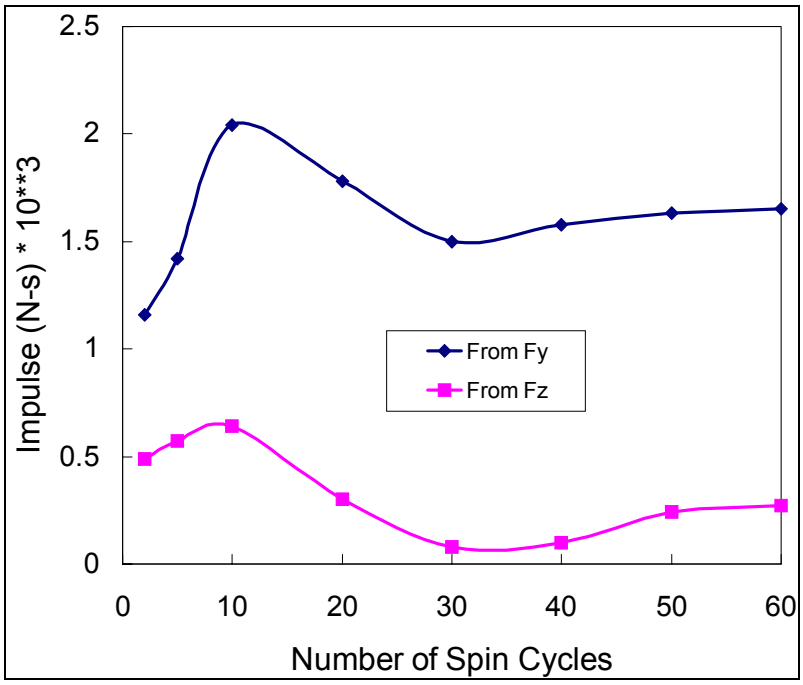

Figure 17. Computed impulse as a function of spin cycles, jet velocity = 69 m/s, LNS, M = 0.24, α = 0 degree, spin = 67 Hz.

The present computed results are currently being used in six-degree-freedom (6-DOF) analyses to determine the feasibility of the synthetic jets to provide control authority for the projectile; the early indications are that they can. Also, a firing test was just recently completed to show that the synthetic jets can provide the control authority needed for maneuvering a subsonic projectile to its target.

4. Summary and Conclusions

This report describes a computational study undertaken to determine the aerodynamic effect of tiny synthetic jets as a means to provide the control authority needed to maneuver a spinning projectile at low subsonic speeds. Computed results have been obtained at a low subsonic speed, M = 0.24 and 0 degree angle of attack, for a subsonic spinning projectile via time-accurate Navier-Stokes computational technique and advanced turbulence models. The unsteady jet is shown in this and earlier studies to substantially alter the flow field near the jet and the base region of the projectile, which in turn affects the forces and moments even at 0 degree angle of attack. It is easier to see the effect of the jet in the RANS predictions for both jets (jet velocities of 31 and 69 m/s). Also, RANS predictions clearly show that the jet effect disappears for the part of the spin cycle when the jet is off. In other words, it reverts to the usual wake without the jet. The level of the lift force predicted by the RANS-LES model is larger than that predicted by the URANS technique. This was also observed earlier in the unsteady calculations for the non-spinning projectile case (*19*).

In general, it is more difficult to easily see the effect of the jet in the unsteady RANS-LES results. Time averaging was required with these unsteady results over many spin cycles. The net time-averaged results obtained over the time period corresponding to one spin cycle clearly show the effect of the synthetic jets on the lift as well as the side forces. It was found that it takes 10 to 20 full spin cycles before the results converge to a periodic state. The effect of the jet in this case is clearly seen when the jet is on during the spin cycle. However, these results show that there is an effect on the lift force (although reduced) for the remainder of the spin cycle when the jet is off. This is a result of the wake effects that persist from one spin cycle to another. The large jet is found to provide larger lift force when the jet is on. The level of lift force for the jet-off period is almost similar. The impulse obtained from the predicted forces for both jets seems to reach an asymptote after 30 spin cycles (the impulse for the larger jet being larger).

This work demonstrates a method to accurately predict the time-accurate unsteady aerodynamics of synthetic jets on an M203 grenade-launched projectile. This capability has provided fundamental understanding of fluid dynamic mechanisms associated with the interaction of the unsteady synthetic jets and the projectile flow fields. The predicted forces and moments are now being used in the 6-DOF simulations to assess if these jets can provide adequate control authority to steer a projectile to its target.

6. References

1. Sahu, J.; Heavey, K. R.; Ferry, E. N. Computational Fluid Dynamics for Multiple Projectile Configurations. *Proceedings of the 3rd Overset Composite Grid and Solution Technology Symposium*, Los Alamos, NM, October 1996.

2. Sahu, J.; Heavey, K. R.; Nietubicz, C. J. Time-Dependent Navier-Stokes Computations for Submunitions in Relative Motion. *6th International Symposium on Computational Fluid Dynamics*, Lake Tahoe, NV, September 1995.

3. Meakin, R. L. *Computations of the Unsteady Flow About a Generic Wing/Pylon/Finned-Store Configuration*; AIAA 92-4568-CP, August 1992.

4. Smith B. L.; Glezer, A. The Formation and Evolution of Synthetic Jets. *Journal of Physics of Fluids* September 1998, 10 (9).

5. Amitay, M.; Kibens, V.; Parekh, D.; Glezer, A. *The Dynamics of Flow Reattachment over a Thick Airfoil Controlled by Synthetic Jet Actuators*; AIAA Paper No. 99-1001, January 1999.

6. Amitay, M.; Smith, D. R.; Kibens, V.; Parekh, D.; Glezer, A. Aerodynamic Flow Control over an Unconventional Airfoil using Synthetic Jet Actuators. *AIAA Journal* **2001**, *39*, 361-370.

7. Davis, S. A.; Glezer, A. *The Manipulation of Large- and Small-Scales in Coaxial Jets using Synthetic Jet Actuators*; AIAA Paper No. 2000-0403, January 2000.

8. He, Y.; Kral, L. *Post-Stall Control on an Airfoil using Localized Jet Actuators*; AIAA Paper No. 2000-0408, January 2000.

9. Lee, C. Y.; Goldstein, D. B. *Two-Dimensional Synthetic Jet Simulation*; AIAA Paper No. 2000-0406, January 2000.

10. Avancha, R.; Pletcher, R. H. *Large Eddy Simulation of the Turbulent Flow Past a Backward Facing Step*; AIAA paper No. 2000-0542, January 2000.

11. Arunajatesan, S.; Sinha, N. *Towards Hybrid LES-RANS Computations of Cavity Flowfields*; AIAA Paper No. 2000-0401, January 2000.

12. Batten, P.; Goldberg U.; Chakravarthy, S. *Sub-grid Turbulence Modeling for Unsteady Flow with Acoustic Resonance*; AIAA Paper 00-0473, 38th AIAA Aerospace Sciences Meeting, Reno, NV, January 2000.

13. Pulliam, T. H.; Steger, J. L. On Implicit Finite-Difference Simulations of Three-Dimensional Flow. *AIAA Journal* **February 1982**, 18 (2), 159–167.

14. Peroomian, O.; Chakravarthy, S.; Goldberg, U. *A 'Grid-Transparent' Methodology for CFD*; AIAA Paper 97-07245, 1997.

15. Peroomian, O.; Chakravarthy, S.; Palaniswamy, S.; Goldberg, U. *Convergence Acceleration for Unified-Grid Formulation Using Preconditioned Implicit Relaxation*; AIAA Paper 98-0116, 1998.

16. Goldberg, U. C.; Peroomian, O.; Chakravarthy, S. A Wall-Distance-Free K-E Model With Enhanced Near-Wall Treatment. *ASME Journal of Fluids Engineering* **1998**, *120*, 457-462.

17. Rinehart, C.; McMichael, J. M.; Glezer, A. *Synthetic Jet-Based Lift Generation and Circulation Control on Axisymmetric Bodies*; AIAA Paper No. 2002-3168.

18. McMichael, J. GTRI, Private Communications

19. Sahu, J. *Unsteady Numerical Simulations of Subsonic Flow over a Projectile with Jet Interaction*; AIAA Paper 2003-1352, Reno, NV, 6-9 January 2003.

NO. OF
COPIES ORGANIZATION

* ADMINISTRATOR
DEFENSE TECHNICAL INFO CTR
ATTN DTIC OCA
8725 JOHN J KINGMAN RD STE 0944
FT BELVOIR VA 22060-6218
*pdf file only

1 DIRECTOR
US ARMY RSCH LABORATORY
ATTN AMSRD ARL CI IS R REC MGMT
2800 POWDER MILL RD
ADELPHI MD 20783-1197

1 DIRECTOR
US ARMY RSCH LABORATORY
ATTN AMSRD ARL CI OK TECH LIB
2800 POWDER MILL RD
ADELPHI MD 20783-1197

1 COMMANDER
NAVAL SURFACE WARFARE CNTR
ATTN CODE B40 DR W YANTA
DAHLGREN, VA 22448-5100

1 COMMANDER
NAVAL SURFACE WARFARE CNTR
ATTN CODE 420 DR A WARDLAW
INDIAN HEAD, MD 20640-5035

1 AIR FORCE ARMAMENT LAB
ATTN AFATL/FXA DAVE BELK
EGLIN AFB FL 32542-5434

3 CDR US ARMY TACOM ARDEC
ATTN AMSTA AR FSF T H HUDGINS
J GRAU W KOENIG
BLDG 382
PICATINNY ARSENAL NJ 07806-5000

1 CDR US ARMY TACOM
ATTN AMSTA AR CCH B
PAUL VALENTI
BLDG 65-S
PICATINNY ARSENAL NJ 07806-5001

1 COMMANDER
US ARMY ARDEC
ATTN SFAE FAS SD MIKE DEVINE
PICATINNY ARSENAL NJ 07806-5001

1 NAVAL AIR WARFARE CENTER
ATTN DAVID FINDLAY
MS 3 BLDG 2187
PATUXENT RIVER MD 20670

NO. OF
COPIES ORGANIZATION

1 UNIV OF ILLINOIS AT URBANA CHAMPAIGN
DEPT OF MECHANICAL AND INDUSTRIAL ENGINEERING
ATTN DR J C DUTTON
URBANA IL 61801

1 CDR US ARMY TACOM-ARDEC
ATTN AMCPM DS MO P BURKE
BLDG 162S
PICATINNY ARSENAL NJ 07806-5000

ABERDEEN PROVING GROUND

1 DIRECTOR
US ARMY RSCH LABORATORY
ATTN AMSRD ARL CI OK (TECH LIB)
BLDG 4600

1 DIR USARL
ATTN AMSRD ARL WM J SMITH
BLDG 4600

1 DIR USARL
ATTN AMSRD ARL WM B W CIEPIELA
BLDG 4600

1 DIR USARL
ATTN AMSRD ARL WM BA D LYON
BLDG 4600

1 DIR USARL
ATTN AMSRD ARL WM BD B FORCH
BLDG 4600

9 DIR USARL
ATTN AMSRD ARL WM BC P PLOSTINS
J DESPIRITO B GUIDOS
K HEAVEY J NEWILL
J SAHU S SILTON
P WEINACHT
BLDG 390

1 DIR USARL
ATTN AMSRD ARL WM BF S WILKERSON
BLDG 390

1 DIR USARL
ATTN AMSRD ARL CI HC R NOAK
BLDG 394